Journal of Ceramic Processing Research. Vol. 12, No. 3, pp. 247~258 (2011)

JOURNAL OF
Ceramic Processing Research

Equivalent circuit model of a $PbZr_{0.6}Ti_{0.4}O_3$ ceramic using impedance spectroscopy

Pramod Chaitanya[a], O. P. Thakur[b], Vinod Kumar[c], Alok Shukla[d] and Lakshman Pandey[e,*]

[a]*NMR and Ceramics Laboratory, Department of Physics & Electronics, Rani Durgavati University, Jabalpur-482001, India*
[b]*Electroceramics Division, Solid State Physics Laboratory, Lucknow Road, Delhi 110054, India*
[c]*Department of Electronics Engineering, Star Academy of Technology & Management, Indore-452010, India,*
[d]*Department of Pure and Applied Physics, Guru Ghasidas University, Bilaspur-495009,India*
[e]*NMR and Ceramics Laboratory, Department of Physics & Electronics, Rani Durgavati University, Jabalpur-482001, India*

The ceramic system $PbZr_{0.6}Ti_{0.4}O_3$ was prepared by a solid state method and impedance measurements were carried out as a function of frequency (100 Hz-10 MHz) in the temperature range 370 K-869 K. Equivalent circuit models that represent the data below and above the transition temperature were arrived at by comparing the experimental plots with the computer-simulated behavior obtained for model circuits. Below the transition temperature the equivalent circuit model comprises a series LCR combination connected in series with a parallel RC network where as for higher temperatures it contains three parallel RC circuits connected in series. Variation of the values of the components as a function of temperature was also studied.

Key words: PZT, Impedance, immittance, modeling, ceramic, equivalent circuit.

Introduction

Piezoelectric ceramics are used in a number of commercial appliances such as microphones and telephone receivers, house hold lighters, accelerometers, pressure sensors, humidity sensors [1] etc. Certain ferroelectric ceramics e.g. perovskites [1, 2] when poled show very strong piezoelectric behavior. Lead zirconate titanate (PZT) is one such material which has been extensively used in commercial devices [3-7]. Due to promises shown by materials having grain sizes in the nanometre range renewed interest is being witnessed for research work in PZT and materials useful in microelectromechanical systems (MEMS) are being further developed to be used as nano-electromechanical system (NEMS). Thus there is enhanced effort in applying PZT in high precision engineering applications such as pressure regulation in micro pumps and high precision positioning devices such as the tip of an electron microscope [8]. This is because PZT actuators offer high resolution down to sub- nanometer range, high stiffness, low wear and tear and fast response times.

As a piezoelectric is usually attached to another system in actual applications, equivalent circuit modeling is found to be very helpful in designing the overall system for optimum power transduction. Over the years a number of equivalent electric circuit models have been developed for PZT/Piezo-ceramics including the Butterworth –Van Dyke model [9-11], Mason model [12], Sherrit *et al.* complex component model [13], constant capacitor model [3], single parallel RC model [3]. Among these models the Butterworth –Van Dyke, Mason's and Sherrit *et al.*'s models have gained high popularity though they represent PZT only in the vicinity of resonance and at temperatures below the transition temperature T_c.

PZT ($PbZr_{1-x}Ti_xO_3$) is a material which is both piezoelectric and ferroelectric and has a phase transition temperature T_c in the range 500 K to 750 K depending upon its composition [1, 2]. An extensive literature is available regarding modeling of PZT at different temperatures [3-7] but, to the best of our knowledge, there seems to be no model reported for PZT ceramics at temperatures ranging from below T_c to above T_c.

In this paper, we present an impedance spectroscopic study of the most popular and vastly used ceramic system, $PbZr_{1-x}Ti_xO_3$(PZT) (x = 0.4) in the frequency range 40 Hz-10 MHz and at temperatures from 370 K to 870 K i.e. below and above T_c (T_c-650 K for this composition). The impedance data is analyzed to obtain equivalent circuit models. In order to facilitate this, the simulated impedance plots are presented for a few model circuits involving RC (resistive and capacitive) and RCL (resistive, capacitive and inductive) elements for quick comparison. In the next section, experimental details of sample preparation and impedance measurements are given which is followed by equivalent circuit modeling, results and discussions.

Models

Equivalent circuit models containing various combinations of resistive (R), capacitive (C), inductive (L) and constant phase angle elements (CPE) have been discussed by different workers [14-28]. Usually use of R's and C's

*Corresponding author:
Tel : +91-761-2609415, +91-761-2605761
Fax: +91-761-2603752
E-mail: pandeyl@hotmail.com

suffice for an electronic ceramic, however for modeling of distributed systems inclusion of CPE and for magnetic and piezoelectric systems inclusion of L's have been found useful. The electrical behavior of a system can be expressed in terms of interrelated functions : impedance ($Z^* = Z' - jZ''$), admittance ($Y^* = (Z^*)^{-1} = Y' + jY''$), permittivity ($\varepsilon^* = (j\omega C_0 Z^*)^{-1} = \varepsilon' - j\varepsilon''$) and modulus ($M^* = (\varepsilon^*)^{-1} = j\omega C_0 Z^* = M' + jM''$) where $j = \sqrt{-1}$ and $\omega = 2\pi f$ with f being the frequency of the ac excitation and C_0 the capacitance of the empty cell used to house the sample. Due to a specific relationship between these broadly termed immittance functions their frequency dependence is utilized to extract information about the components used in the models and hence about the behavior of the system. It has been reported that a study of the ceramic systems based on the information conveyed by only one of these four functions does not suffice and two functions viz. impedance (Z^*) and modulus (M^*) or admittance (Y^*) and permittivity (ε^*) should be looked at [19-21]. In certain cases more than two immittance functions might need to be looked at.

The selection of the most probable model is facilitated by comparing the experimentally -observed behavior with simulated immittance plots corresponding to different models. Computer programs are used for this purpose using graphics. In what follows, a brief overview of the modeling is presented. Also simulated spectra of the models found to be the most useful for the ceramic system are presented for a ready reference. Detailed treatment of various models can be found in reference [27].

Models containing RC only

Models involving a number of RC combinations are possible and several of them have been used in the literature [14-27]. In the present paper, models containing only one, two and three RC's are discussed to elaborate the process of modeling.

One RC circuit

A RC circuit has one time constant and can be conveniently used to represent one charge transfer/relaxation process in the material. This is the simplest realistic model that can be utilized to represent the electrical behavior of a material. It has been used to represent piezoelectrics also [3]. The real and imaginary parts of the complex impedance $Z^* = Z' - jZ''$ of a parallel RC combination (Fig. 1(a)) are given by:

$$Z' = \frac{R_{11}}{1+(\omega C_{11} R_{11})^2} \tag{1}$$

$$Z'' = \frac{\omega C_{11} R_{11}^2}{1+(\omega C_{11} R_{11})^2} \tag{2}$$

Real and imaginary part of the modulus M^* are given as:

$$M' = \omega C_0 \left(\frac{\omega C_{11} R_{11}^2}{1+(\omega C_{11} R_{11}^2)^2} \right) \tag{3}$$

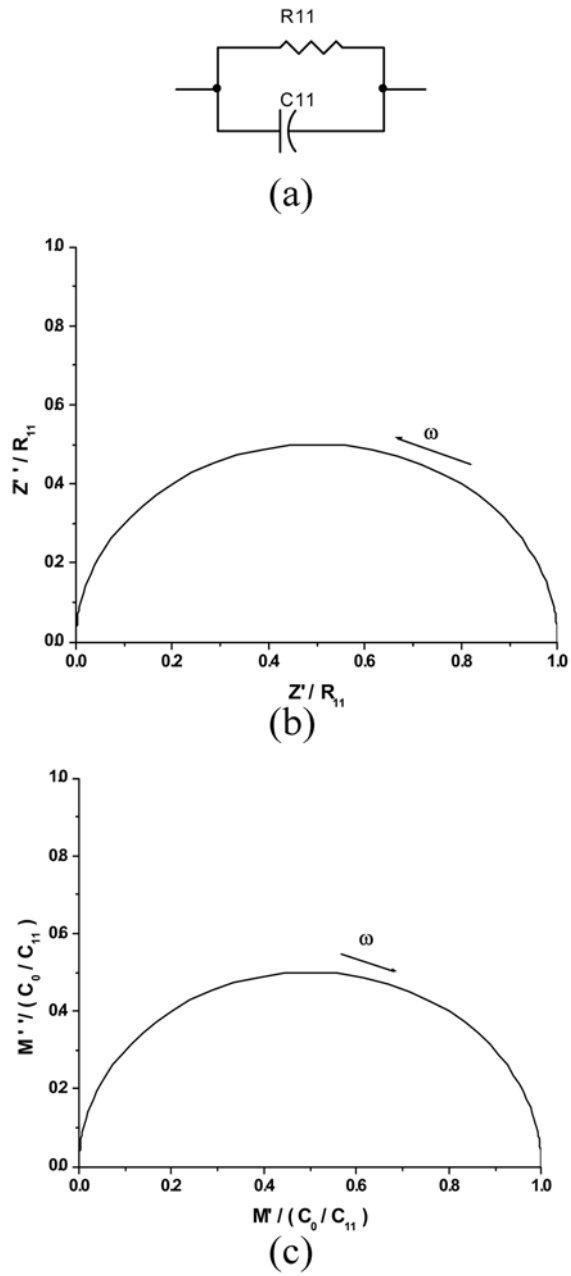

Fig. 1. (a) Model comprising parallel combination of resistor (R_{11}) and capacitor (C_{11}).
Normalized plots (b) Z''/R_{11} vs. Z'/R_{11} and (c) $M''(C_{11}/C_0)$ vs. $M'(C_{11}/C_0)$, for Model shown in Fig 1(a).

$$M'' = \omega C_0 \left(\frac{R_{11}}{1+(\omega C_{11} R_{11})^2} \right) \tag{4}$$

The limiting values at $\omega \to 0$ and $\omega \to \infty$ are as given below:

$$Z'|_{\omega\to 0} = R_{11} \qquad Z'|_{\omega\to\infty} = R_{11}$$

$$Z''|_{\omega\to 0} = 0 \qquad Z''|_{\omega\to\infty} = 0$$

$$M''|_{\omega\to 0} = 0 \qquad M''|_{\omega\to\infty} = \frac{C_0}{C_{11}}$$

$$M''|_{\omega\to 0} = 0 \qquad M''|_{\omega\to\infty} = 0 \tag{5}$$

It is seen that Z′ and Z″ given in Eq. 1 & 2 satisfy the relation:

$$(Z' - R_{11}/2)^2 + Z''^2 = (R_{11}/2)^2 \quad (6)$$

which is the equation of a circle with center at (R_{11}/2,0) and radius equal to $R_{11}/2$. As Z′ and Z″ are positive quantities this plot is actually a semicircle. The point ($Z' = R_{11}$, $Z = 0$) corresponds to $\omega = 0$ i.e. dc resistance. Thus the curve of the Z″ vs. Z′ plot intercepts the Z′ axis at R_{11} at the low frequency end. The maximum value of Z″ occurs when $\omega R_{11} C_{11} = 1$. By knowing the frequency at which the maximum value of Z″ occurs, the value of C_{11} can be obtained. The value of C_{11} can also be obtained by looking at the M plots. M′ and M″ as given in Eq. 3 & 4 satisfy the relation:

$$(M' - C_0/2C_{11})^2 + M''^2 = (C_0/2C_{11})^2 \quad (7)$$

As $\omega \to 0$, $M' = 0$ and $M'' = 0$ and at $\omega \to \infty$, $M' = C_0/C_{11}$ and $M'' = 0$ indicating that a M″ vs. M′ plot would be a semicircular arc with a center at ($C_0/2C_{11}$,0) and a high frequency intercept on the M′ axis at C_0/C_{11}. Thus knowledge of C_0 yields the value of C_{11}. Normalized plots of Z″ vs. Z′ and M″ vs. M′ are shown in Figs. 1(b) and 1(c).

It may be mentioned that as series and parallel representations are equivalent a series RC circuit may also be chosen as a model. The Z and M plots would be just vertical lines and would not carry much information. However Y and ε plots would be circular arcs and hence could be used to extract information [19]. The choice of series or parallel combinations can be made by looking at the experimental immittance plots. Also for ease of mathematical treatment the RC network can be replaced by a capacitor with a complex dielectric constant [3].

Two RC circuits

When two charge transfer processes are present in the material, a series combination of two parallel RC circuits having time constants $R_{11}C_{11}$ and $R_{12}C_{12}$ may be considered as a representative model, as shown in Fig 2(a), to start with. Real and imaginary parts of Z* and M* are given by Eq.8-11 :

$$Z' = \frac{R_{11}}{1+(\omega C_{11}R_{11})^2} + \frac{R_{12}}{1+(\omega C_{12}R_{12})^2} \quad (8)$$

$$Z'' = \frac{\omega C_{11}R_{11}^2}{1+(\omega C_{11}R_{11})^2} + \frac{\omega C_{12}R_{12}^2}{1+(\omega C_{12}R_{12})^2} \quad (9)$$

$$M' = \omega C_0 \frac{R_{11}}{1+(\omega C_{11}R_{11})^2} + \frac{R_{12}}{1+(\omega C_{12}R_{12})^2} \quad (10)$$

$$M'' = \omega C_0 \frac{R_{11}}{1+(\omega C_{11}R_{11})^2} + \frac{R_{12}}{1+(\omega C_{12}R_{12})^2} \quad (11)$$

The limiting values at $\omega \to 0$ and $\omega \to \infty$ are given below:

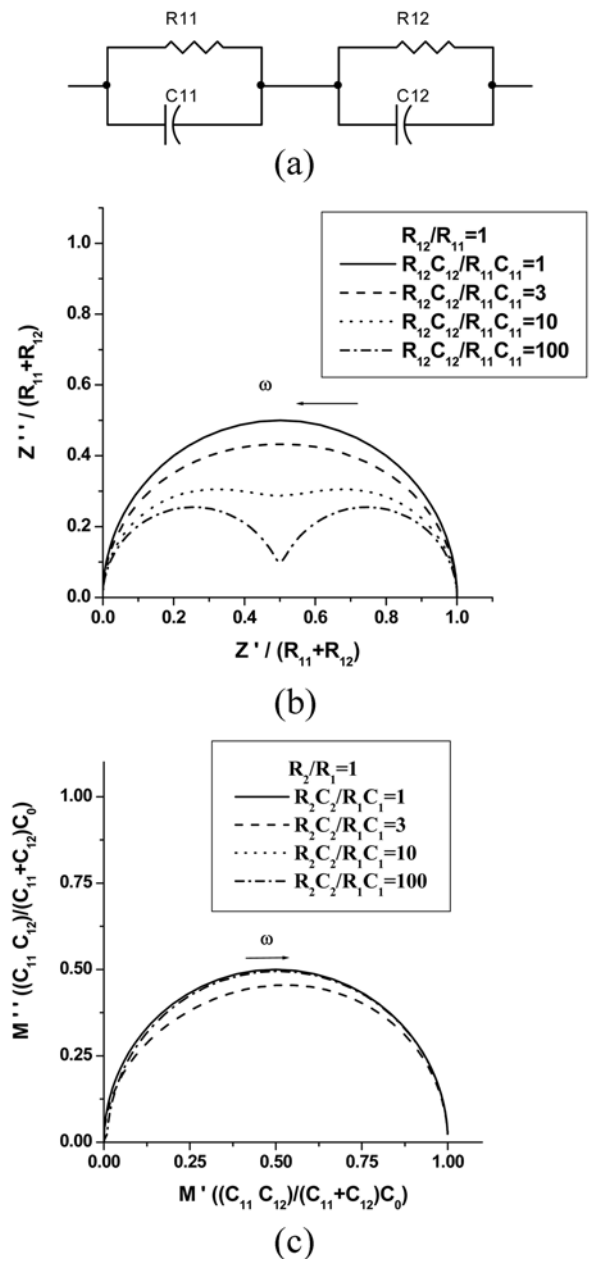

Fig. 2. (a) Model comprising two parallel RC circuits in series. Normalized plots (b) Z"/($R_{11} + R_{12}$) vs. Z'/($R_{11} + R_{12}$) and (c) M" ((C_{11} C_{12})/C_0($C_{11} + C_{12}$)) vs. M' ((C_{11} C_{12})/C_0($C_{11} + C_{12}$)) for the model shown in Fig. 2(a).

$$Z'|_{\omega\to 0} = R_{11} + R_{12} \qquad Z'|_{\omega\to\infty} = 0$$

$$Z''|_{\omega\to 0} = 0 \qquad Z''|_{\omega\to\infty} = 0$$

$$M''|_{\omega\to 0} = 0 \qquad M''|_{\omega\to\infty} = C_0\left(\frac{C_{11}+C_{12}}{C_{11}C_{12}}\right)$$

$$M''|_{\omega\to 0} = 0 \qquad M''|_{\omega\to\infty} = 0 \quad (12)$$

Typical plots of this model for Z″ vs. Z′ and M″ vs. M′ are shown in Fig. 2(b-c).

As is shown in Fig. 2 the Z″ vs. Z′ plot may contain two distinct arcs or may appear slightly depressed depending upon the ratios $R_{12}C_{12}/R_{11}C_{11}$ and R_{12}/R_{11}. A slightly

depressed semicircular arc indicates the presence of a distribution of the time constant or the presence of at least two processes whose time constants are close to each other within a factor 3 [see Fig 2(b)]. The simulated plots for various values of the ratios of time constants and of resistances are given in reference [19]. Few plots are reproduced here for a ready reference. For certain ratios of time constants M plots would have more features than Z plots and would be more useful. It may be further mentioned that if C_{12} is extremely small such that the parallel combination $R_{12}C_{12}$ approaches R_{12} only, then Z″ vs. Z′ is still a semicircular arc but the plot gets shifted by R_{12} to right on the Z′ axis and the M″ vs. M′ plot shows a steeply rising branch at the high frequency side. Similarly if R_{12} is extremely large such that the parallel combination $R_{12}C_{12}$ approaches C_{12} only, then the Z″ vs. Z′ plot shows a steeply rising branch at the low frequency end and the M″ vs. M′ plots gets shifted on the M′ axis. These results are found to be very useful in choosing the models. If an experimental Z″ vs. Z′ plot shows a shift and a M″ vs. M′ plot a steeply rising branch then the presence of a series resistance in the model is inferred and if the M″ vs. M′ plot is shifted and the Z″ vs. Z′ plot shows a steeply rising branch then the presence of a series capacitance is inferred.

Three RC circuits

When three charge transfer processes are present as is usually the case with a ceramic-electrode system (a ceramic-electrode system can be thought of as a grain -grain boundary- electrode system), a model comprising three parallel RC circuits connected in series as shown in Fig. 3(a) can be chosen to start with. Real and imaginary parts of Z* and M* are given by Eq. 13-16:

$$Z' = \frac{R_{11}}{1+(\omega C_{11}R_{11})^2} + \frac{R_{12}}{1+(\omega C_{12}R_{12})^2} + \frac{R_{13}}{1+(\omega C_{13}R_{13})^2} \quad (13)$$

$$Z'' = \frac{\omega C_{11}R_{11}^2}{1+(\omega C_{11}R_{11})^2} + \frac{\omega C_{12}R_{12}^2}{1+(\omega C_{12}R_{12})^2} + \frac{\omega C_{13}R_{13}^2}{1+(\omega C_{13}R_{13})^2} \quad (14)$$

$$M' = \omega C_0 \frac{\omega C_{11}R_{11}^2}{1+(\omega C_{11}R_{11})^2} + \frac{\omega C_{12}R_{12}^2}{1+(\omega C_{12}R_{12})^2} + \frac{\omega C_{13}R_{13}^2}{1+(\omega C_{13}R_{13})^2} \quad (15)$$

$$M'' = \omega C_0 \frac{R_{11}}{1+(\omega C_{11}R_{11})^2} + \frac{R_{12}}{1+(\omega C_{12}R_{12})^2} + \frac{R_{13}}{1+(\omega C_{13}R_{13})^2} \quad (16)$$

The limiting values at $\omega \to 0$ and $\omega \to \infty$ are given below:

$$Z'|_{\omega\to 0} = R_{11} + R_{12} + R_{13} \qquad Z'|_{\omega\to\infty} = 0$$

$$Z''|_{\omega\to 0} = 0 \qquad Z''|_{\omega\to\infty} = 0$$

$$M'|_{\omega\to 0} = 0 \qquad M'|_{\omega\to\infty} = C_0\left(\frac{1}{C_{11}} + \frac{1}{C_{12}} + \frac{1}{C_{13}}\right)$$

$$M''|_{\omega\to 0} = 0 \qquad M''|_{\omega\to\infty} = 0 \quad (17)$$

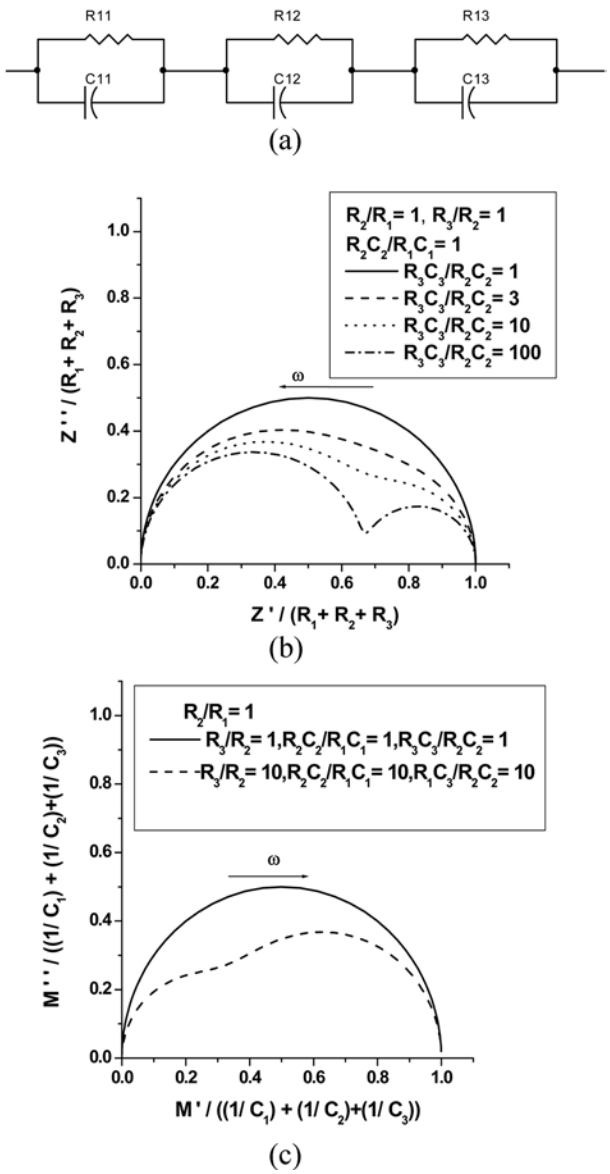

Fig. 3. (a) Model comprising three parallel RC circuits connected in series.
Normalized plots (b) Z"/(R_{11} + R_{12} + R_{13}) vs. Z'/(R_{11} + R_{12} + R_{13}) (c) M"/(1/C_{11}+ 1/C_{12}+ 1/C_{12}) vs. M'/(1/C_{11} + 1/C_{12} + 1/C_{12}) for the model shown in Fig. 3(a).

Typical plots of Z″ vs. Z′ and M″ vs. M′ for this model are shown in Fig. 3(b-c). It may be noted that skewed shapes arise due to different ratios of time constants and resistances. For widely separated values of time constants and resistances three joined semicircular arcs appear.

Inclusion of inductive component L

The impedance behavior of materials in general can be modeled by using RC networks connected in ways indicated by the presence of various polarization processes. However when the material is magnetic, the energy stored in it will be magnetic in nature. In an electric circuit, the inductor stores energy in the form of a magnetic field. Thus an equivalent circuit model involving an inductance 'L' would

be convenient for a magnetic system. Models consisting of resistance 'R' and inductance 'L' have been studied in detail by Katare *et al* [18, 21]. Since a vibrating damped spring mass system can be mathematically treated in the same way as a driven LCR circuit and a piezoelectric sample executes mechanical vibrations when stressed by an externally applied ac field, a piezoelectric also can be modeled by using inductors together with resistances and capacitances [1, 2, 28, 29]. Here we present few models relevant to our work and their simulated behavior so that a suitable model for our PZT could be arrived at by comparison. As models containing inductors with capacitors have not been explored much from the point- of- view of applications to electronic ceramics, we give here expressions for all the four immittance functions with some plots.

A series RLC circuit

A model comprising a series combination of R, L and C is shown in Fig 4(a). Real and imaginary parts of immittance functions for this model are given by Eq. 18-25:

$$Z' = R_{11} \tag{18}$$

$$Z'' = \left(\frac{1}{\omega C_{11}} - \omega L_{11}\right) \tag{19}$$

$$M' = C_0\left(\frac{1}{C_{11}} - \omega^2 L_{11}\right) \tag{20}$$

$$M'' = \omega C_0 R_{11} \tag{21}$$

$$Y' = \frac{\omega^2 C_{11}^2 R_{11}}{\omega^2 R_{11}^2 C_{11}^2 + 1 + \omega^4 L_{11}^2 C_{11}^2 - 2\omega^2 L_{11} C_{11}} \tag{22}$$

$$Y'' = \frac{\omega C_{11} - \omega^3 C_{11}^2 R_{11}}{\omega^2 R_{11}^2 C_{11}^2 + 1 + \omega^4 L_{11}^2 C_{11}^2 - 2\omega^2 L_{11} C_{11}} \tag{23}$$

$$\varepsilon' = \frac{1}{C_0}\left[\frac{C_{11} - \omega^2 C_{11}^2 L_{11}}{1 + \omega^2 R_{11}^2 C_{11}^2 + \omega^4 L_{11}^2 C_{11}^2 - 2\omega^2 L_{11} C_{11}}\right] \tag{24}$$

$$\varepsilon'' = \frac{1}{C_0}\left[\frac{C_{11}^2 R_{11}}{\omega^2 R_{11}^2 C_{11}^2 + 1 + \omega^4 L_{11}^2 C_{11}^2 - 2\omega^2 L_{11} C_{11}}\right] \tag{25}$$

Limiting values of these are given below:

$$Z'|_{\omega\to 0} = R_{11} \qquad Z'|_{\omega\to\infty} = R_{11}$$
$$Z''|_{\omega\to 0} = -\infty \qquad Z''|_{\omega\to\infty} = +\infty$$
$$M'|_{\omega\to 0} = \frac{C_0}{C_{11}} \qquad M'|_{\omega\to\infty} = -\infty$$
$$M''|_{\omega\to 0} = 0 \qquad M''|_{\omega\to\infty} = \infty$$
$$Y'|_{\omega\to 0} = 0 \qquad Y'|_{\omega\to\infty} = 0$$
$$Y''|_{\omega\to 0} = 0 \qquad Y''|_{\omega\to\infty} = 0$$
$$\varepsilon'|_{\omega\to 0} = \frac{C_{11}}{C_0} \qquad \varepsilon'|_{\omega\to\infty} = 0$$
$$\varepsilon''|_{\omega\to 0} = 0 \qquad \varepsilon''|_{\omega\to\infty} = 0 \tag{26}$$

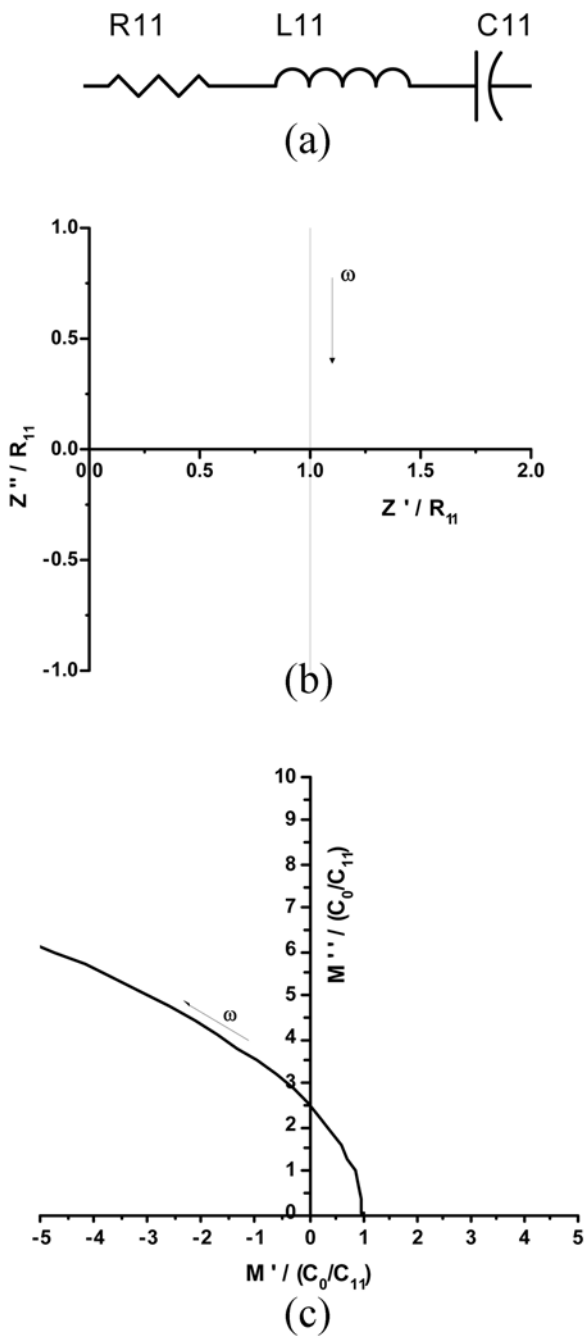

Fig. 4. (a) Model having a series combination of R, L and C. Normalized plot of (b) Z''/R_{11} vs. Z'/R_{11}; (c) $M''/(C_0/C_{11})$ vs. $M'/(C_0/C_{11})$ for model shown in Fig. 4(a).

The simulated complex plane plots for Z and M are shown in Fig. 4(b-c).

The resonance frequency ω_r, of the model is obtained by equating the imaginary part of the impedance to zero and is given by:

$$\omega_r = \sqrt{\frac{1}{L_{11} C_{11}}} \tag{27}$$

The values of R_{11}, C_{11} and L_{11} can be obtained from the

limiting values of Z' and M' at $\omega \to 0$ and using the relation $L_{11} = 1/(\omega_r^2 C_{11})$. Further, it is seen that $M'(= \omega C_0 Z'')$ will be equal to zero when Z'' becomes zero i.e. at the resonance frequency ω_r. The corresponding value of M'' would be given by $M'' = C_0\, \omega_r\, R_{11}$ and this corresponds to the intercept of the M'' vs. M' curve with the M'' axis. This value of M'' can further be written as:

$$M'' = \frac{C_0}{C_{11}} \frac{C_{11} R_{11}}{\sqrt{\frac{L_{11}}{R_{11}} \cdot R_{11} C_{11}}} \tag{28}$$

or:

$$M''\left(\frac{C_0}{C_{11}}\right)^{-1} = \frac{R_{11} C_{11}}{\sqrt{\frac{L_{11}}{R_{11}} \cdot R_{11} C_{11}}} = \sqrt{\frac{R_{11} C_{11}}{\frac{L_{11}}{R_{11}}}} = \sqrt{\frac{\tau_C}{\tau_L}} \tag{29}$$

where τ_C and τ_L are the time constants for capacitive and inductive components. A value greater than 1 for this ratio means that the capacitive part is responding slowly as compared to the inductive part. The value of L can also be estimated by Eq. 29 where C_0, C_{11}, R_{11}, and M'' (the value of the intercept of M'' vs. M' plot on the M'' axis) are known here. Also it can be shown that the values of M' and M'' satisfy the equation:

$$M''^2 = \frac{(C_0 R_{11})^2}{C_0 L_{11}} \left[\frac{C_0}{C_{11}} - M'\right] \tag{30}$$

this is the equation of a parabola of the type $y^2 = 4a\,(x - x_0)$ where the terms have usual meaning.

It is to be mentioned that this behavior is clearly seen in the simulated plots as is shown in Fig. 4(c). It is also found that Y' and Y'' satisfy the following relation:

$$\left(Y' - \frac{1}{2R_{11}}\right)^2 + Y''^2 = \left(\frac{1}{2R_{11}}\right)^2 \tag{31}$$

which represents a circle of radius $\frac{1}{2R_{11}}$ and centre at $\left(\frac{1}{2R_{11}}, 0\right)$.

Eq. 31 can be used to obtain the value of R_{11}. Values of these components can be obtained from other immittance functions also. These plots are not being given here. Applications of admittance plots to obtain values of components has been discussed by Sheritt *et al.* and others [13, 30].

A series RLC circuit in parallel to another C

A series combination of R_{11}, L_{11} and C_{11} in parallel to C_{12} is shown in Fig. 5(a). This is the so-called Van Dyke model [9-11] and is the most widely used model to represent a pie-

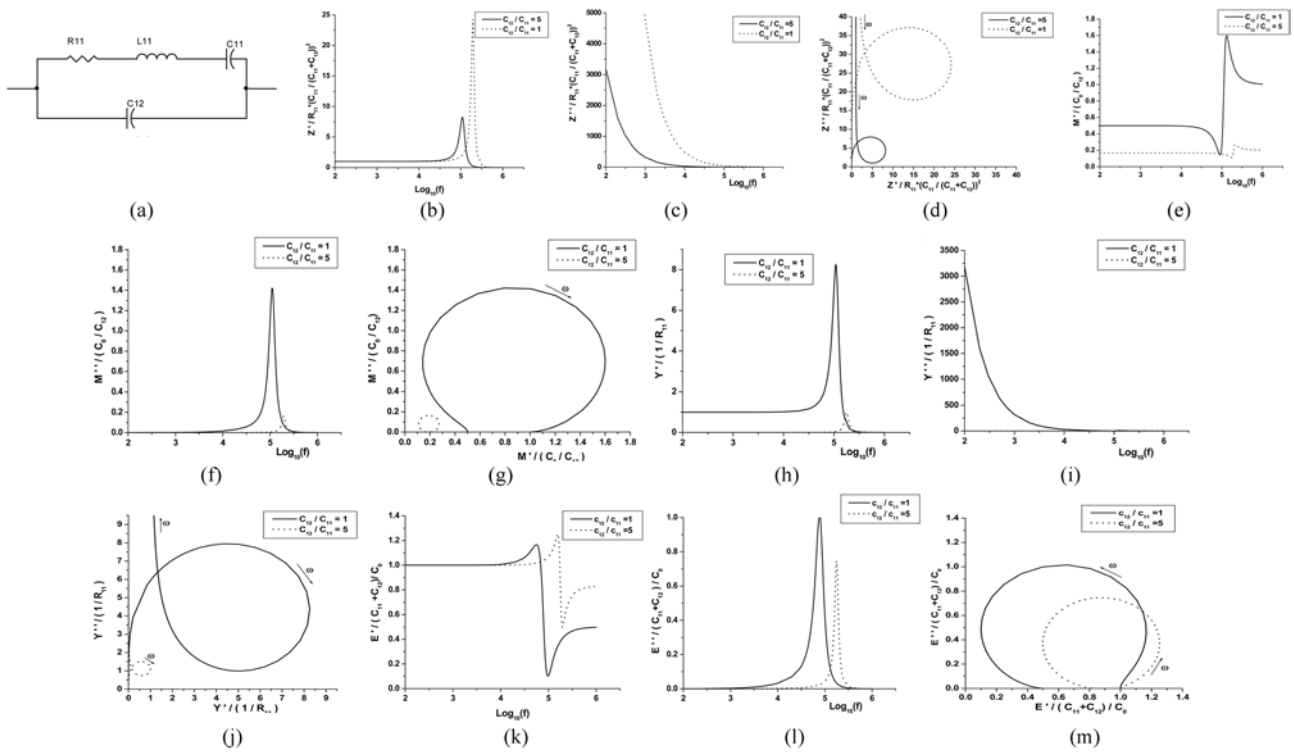

Fig. 5. (a) Model having a series RLC circuit in parallel to another C.
Normalized Plots (b) $Z'/R_{11} * (C_{11}/(C_{11} + C_{12}))^2$ vs. Log_{10} (F); (c) $Z''/R_{11} * (C_{11}/(C_{11} + C_{12}))^2$ vs. Log_{10} (F); (d) $Z''/R_{11} * (C_{11}/(C_{11} + C_{12}))^2$ vs. $Z'/R_{11} * (C_{11}/(C_{11} + C_{12}))^2$ for model shown in Fig. 5(a).
Normalized Plots (e) $M'/(C_0/C_{12})$ vs. Log_{10} (F); (f) $M''/(C_0/C_{12})$ vs. Log_{10} (F) (g) $M''/(C_0/C_{12})$ vs. $M'/(C_0/C_{12})$ for model shown in Fig. 5(a).
Normalized Plots (h) $Y'/(1/R_{11})$ vs. Log_{10} (F); (i) $Y''/(1/R_{11})$ vs. Log_{10} (F); (j) $Y''/(1/R_{11})$ vs. $Y'/(1/R_{11})$ for model shown in Fig. 5(a).
Normalized Plots (k) $\varepsilon'/((C_{11} + C_{12})/C_0)$ vs. Log_{10} (F) (l) $\varepsilon''/((C_{11} + C_{12})/C_0)$ vs. Log_{10} (F); (m) $\varepsilon''/((C_{11} + C_{12})/C_0)$ vs. $\varepsilon'/((C_{11} + C_{12})/C_0)$ for model shown in Fig. 5(a).

zoelectric. Therefore for this case we give below expressions and complex plane plots of all the immittance functions:

$$Z' = \frac{R_{11}}{\left[1-\omega C_{12}\left(\omega L_{11}-\frac{1}{\omega C_{11}}\right)\right]^2+[\omega C_{12}R_{11}]^2} \quad (32)$$

$$Z'' = \frac{\omega C_{12}R_{11}^2-\left(\omega L_{11}-\frac{1}{\omega C_{11}}\right)+\left(\omega L_{11}-\frac{1}{\omega C_{11}}\right)^2\omega C_{12}}{\left[1-\omega C_{12}\left(\omega L_{11}-\frac{1}{\omega C_{11}}\right)\right]^2+[\omega C_{12}R_{11}]^2} \quad (33)$$

$$Y' = \frac{R_{11}}{R_{11}^2+\left(\omega L_{11}-\frac{1}{\omega C_{11}}\right)^2} \quad (34)$$

$$Y'' = \frac{-\left(\omega L_{11}-\frac{1}{\omega C_{11}}\right)}{R_{11}^2+\left(\omega L_{11}-\frac{1}{\omega C_{11}}\right)^2}+\omega C_{12} \quad (35)$$

$$M' = \omega C_0\left(\frac{\omega C_{12}R_{11}^2-\left(\omega L_{11}-\frac{1}{\omega C_{11}}\right)+\left(\omega L_{11}-\frac{1}{\omega C_{11}}\right)^2\omega C_{12}}{\left[1-\omega C_{12}\left(\omega L_{11}-\frac{1}{\omega C_{11}}\right)\right]^2+[\omega C_{12}R_{11}^2]}\right) \quad (36)$$

$$M'' = \frac{\omega C_0 R_{11}}{\left[1-\omega C_{12}\left(\omega L_{11}-\frac{1}{\omega C_{11}}\right)\right]^2+[\omega C_{12}R_{11}^2]} \quad (37)$$

$$\varepsilon' = \frac{C_{12}}{C_0}-\frac{\left(\omega L_{11}-\frac{1}{\omega C_{11}}\right)}{\omega C_0\left[R_{11}^2+\left(\omega L_{11}-\frac{1}{\omega C_{11}}\right)^2\right]} \quad (38)$$

$$\varepsilon'' = \frac{R_{11}}{\omega C_0\left[R_{11}^2+\left(\omega L_{11}-\frac{1}{\omega C_{11}}\right)^2\right]} \quad (39)$$

Limiting values of these are given by:

$$Z'|_{\omega\to 0} = \left(\frac{C_{11}}{C_{11}+C_{12}}\right)^2 R_{11} \qquad Z'|_{\omega\to\infty} = 0$$

$$Z''|_{\omega\to 0} = \infty \qquad Z''|_{\omega\to\infty} = 0$$

$$M'|_{\omega\to 0} = \left(\frac{C_{11}}{C_{11}+C_{12}}\right) \qquad M'|_{\omega\to\infty} = \frac{C_0}{C_{12}}$$

$$M''|_{\omega\to 0} = 0 \qquad M''|_{\omega\to\infty} = 0$$

$$Y'|_{\omega\to 0} = 0 \qquad Y'|_{\omega\to\infty} = \frac{1}{R_{11}}$$

$$Y''|_{\omega\to 0} = \infty \qquad Y''|_{\omega\to\infty} = 0$$

$$\varepsilon'|_{\omega\to 0} = \left(\frac{C_{11}+C_{12}}{C_0}\right) \qquad \varepsilon'|_{\omega\to\infty} = \frac{C_{12}}{C_0}$$

$$\varepsilon''|_{\omega\to 0} = 0 \qquad \varepsilon''|_{\omega\to\infty} = 0 \quad (40)$$

Simulated plots are shown in Fig. 5(b-m).

Experimental

The sample with a composition $PbZr_{0.6}Ti_{0.4}O_3$ was prepared by a solid state ceramic method using powdered PbO, ZrO_2 and TiO_2 (AR grade, purity better than 99%) as starting materials. Excess PbO (2 mol%) was taken to compensate the lead loss during sintering at elevated temperatures. An appropriate amount of the mixture was placed in a zirconia pot with 10 zirconia balls of 15 mm diameter and was subjected to grinding using a planetary ball mill for two hours. The ground product was calcined at 800 °C for 4 hours. The powder was ball-milled again and calcined at 850 °C for 4 hours. The formation of a single phase was checked by X-ray diffraction (XRD) analysis using a Phillips diffractometer, 3200 with Cu-Kα radiation. The synthesized powder were pressed into disks of 10 mm diameter and then sintered in an air atmosphere for 4 hours at 1200 °C. For the electrical measurements, sintered pellets were ground to a thickness of 0.4 mm. Both the parallel faces of the sample were polished and sputtered by gold serving as electrodes. Measurements of the real and imaginary parts of the impedance (Z*) as a function of the frequency (40 Hz-10 MHz) in the temperature range 370 K-869 K was carried out using an HP-4194A impedance analyzer interfaced with a computer. A delay of 100 ms was introduced between two frequencies. Heating was maintained at 1 K·minute^{-1} and data were recorded automatically. These data were used to determine the real and imaginary parts of other complex immittance functions viz. admittance ($Y^* = 1/Z^* = Y' + jY''$), dielectric modulus ($M^* = j\omega C_0 Z^* = M' + jM''$) and permittivity ($\varepsilon^* = (j\omega C_0 Z^*)^{-1} = \varepsilon' - j\varepsilon''$). It has been reported that a study of ceramics based on the information carried out by only one of these four functions does not suffice and two functions viz. impedance (Z*) and dielectric modulus (M*) or admittance (Y*) and permittivity (ε*) should be considered [18, 19]. Therefore in the present study, impedance and modulus data were used to find out the equivalent circuit models that represent the electrical behavior of the system $PbZr_{0.6}Ti_{0.4}O_3$ (PZT) best. Values of different resistive (R's), capacitive (C's) and inductive (L's) components of the modeled equivalent circuits were determined by a complex nonlinear least squares (CNLS) fitting program using IMPSPEC.BAS software developed by Pandey [31].

Results, Analysis of Data and Discussion

Typical experimental plots for Z* and M* at different temperatures (699 K, 793 K and 869 K) above T_c (T_c is near 650 K for this composition) are shown in Figs. 6-8. Plots for temperature 538 K (i.e. below T_c) are shown in Fig. 9. Plots for lower temperatures are similar to this and are not shown. In all these figures the experimental data are shown by dark points.

With a closer look at the experimental plots (dark points) shown in Figs. 6-9, it is clear that the behaviors of the ceramic system $PbZr_{0.6}Ti_{0.4}O_3$ (PZT) at temperatures below

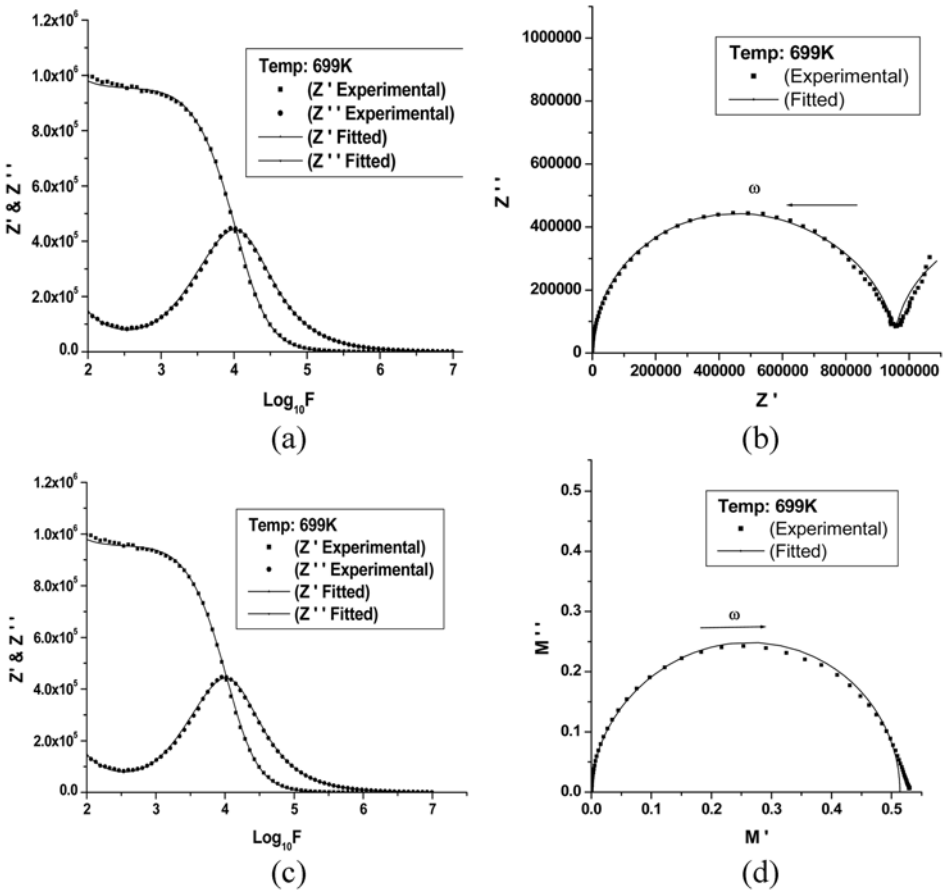

Fig. 6. Experimental and fitted plots for 699 K (a) Z' & Z'' vs. $Log_{10}F$; (b) Z'' vs. Z'.
Experimental and fitted plots for 699K (c) M' & M'' vs. $Log_{10}F$; (d) M'' vs. M'.

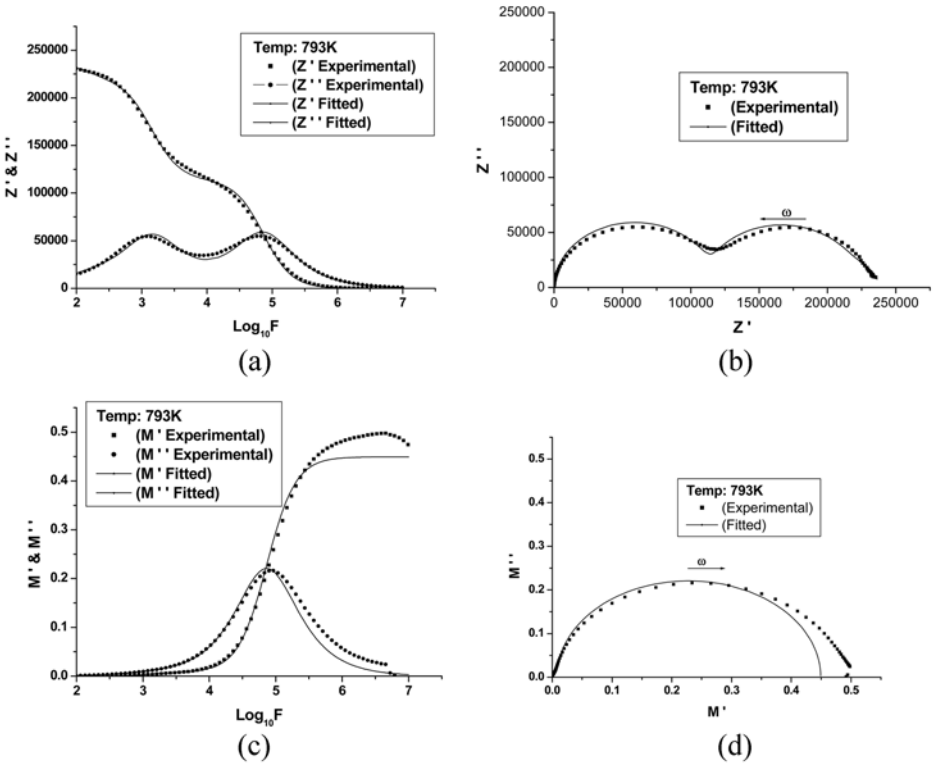

Fig. 7. Experimental and fitted plots for 793 K (a) Z' & Z'' vs. $Log_{10}F$; (b) Z'' vs. Z'.
Experimental and fitted plots for 793 K (c) M' & M'' vs. $Log_{10}F$; (d) M'' vs. M'.

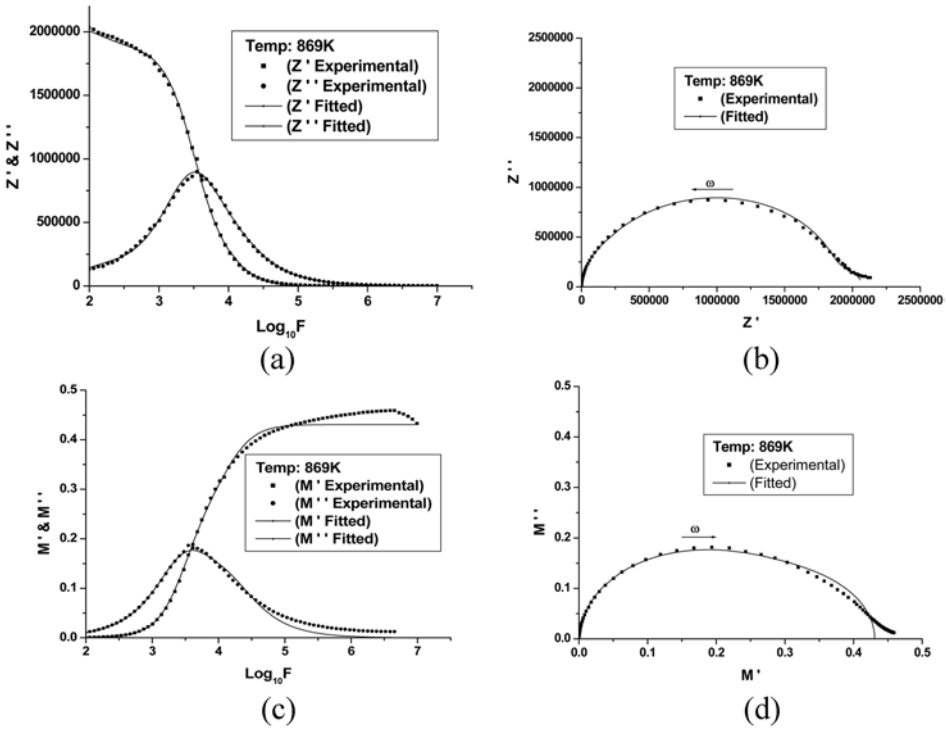

Fig. 8. Experimental and fitted plots for 869 K (a) Z' & Z'' vs. $Log_{10}F$; (b) Z'' vs. Z'. Experimental and fitted plots for 869 K (c) M' & M'' vs. $Log_{10}F$; (d) M'' vs. M'.

T_c and above T_c are different as expected. Therefore there should be two different models to represent PZT in these temperature ranges.

A quick look at Figs. 6-8 reveals that there are no steeply rising branches or shifts in the Z* and M* plots in the complex plane. This indicates that the equivalent circuit model would not contain a series R or series C since the presence of a series R would give rise to a shift in the Z″ vs. Z′ plot and a steeply rising high frequency branch in the corresponding M″ vs. M′ plot. Similarly the presence of a series C would give rise to a shift in the M″ vs. M′ plot and a steeply rising low frequency branch in the corresponding Z″ vs. Z′ plots as discussed in previous sections.

As a ceramic system, in general, would possess grain, grain-boundary and electrode processes and the material $PbZr_{0.6}Ti_{0.4}O_3$ (PZT) under consideration would no longer be a piezoelectric above T_c , it may be modeled by three parallel RC circuits R_1C_1, R_2C_2 and R_3C_3 representing these processes and connected in series to start with. By drawing three tentative semicircular connected arcs corresponding to these in Fig. 6(b), Fig. 7(b), Fig. 8(b), and comparing these with simulated plots of model shown in Fig. 3(a) the values of R_1, C_1, R_2, C_2, R_3, and C_3 were obtained by the intercepts of the arcs on the Z′ axis and the frequencies where Z″ would show peaks. Values thus estimated are $4.9 \times 10^5\ \Omega$, 1.20×10^{-10} F, $4.9 \times 10^5\ \Omega$, 4.67×10^{-12} F, $10.2 \times 10^5\ \Omega$, 3.98×10^{-9} F for 699 K; $0.7 \times 10^5\ \Omega$, 6.86×10^{-12} F, $0.6 \times 10^5\ \Omega$, 5.44×10^{-9} F, $1.1 \times 10^5\ \Omega$, 1.04×10^{-11} F for 793 K and $8.0 \times 10^5\ \Omega$, 2.11×10^{-10} F, $8.0 \times 10^5\ \Omega$, 7.99×10^{-12} F, $5.5 \times 10^5\ \Omega$, 1.44×10^{-12} F for 869 K.

The exact values of R_1, C_1, R_2, C_2, R_3 and C_3 were obtained by fitting the experimental data to expressions of Z′ and Z″ given by Eq. 13 & 14 for this model by using complex non-linear least squares (CNLS) fitting and are given in Table 1. The software "IMPSPEC.BAS" developed in our laboratory [31] and applied earlier for several systems [18-27] was used and the estimated values given above were taken as initial guesses.

Now let us look at the behavior at temperature below T_c. The Z″ vs. Z′ plot at 538 K (see Fig. 9(b)) is nearly a straight line parallel to the Y-axis and does not yield much information. The M″ vs. M′ plot is as shown in Fig. 9(c). Here the plot seems to be a curve that starts from a point on the M′ axis, turns towards the M″ axis, intercepts it and then rises up. This is clearly visible in the inset of Fig. 9(c) where the scales have been changed so that this pattern is highlighted. Comparing these plots with the simulated plots shown in a previous section, it is seen that the experimental plot shown in Fig. 9(c) is somewhat similar to the simulated plot of Fig. 4(c) which corresponds to the series LCR circuit shown in Fig. 4(a). It was thus inferred that the equivalent circuit model would contain a series L_1, C_1, R_1 circuit. The value of C_1 was estimated from the low frequency intercept of the M″ vs. M′ arc with the M′ axis by using $M'|_{\omega \to 0} = C_0/C_1$. The value of L_1 was obtained from the frequency where the M″ vs. M′ arc cuts the M″ axis (this point corresponds to Z″ = 0 and M′ = 0 i.e. resonance) and the value of C_1 by using $\omega_r = \sqrt{1/L_{11}C_{11}}$ (see Eq. 27 where L_{11} and C_{11} are replaced

Table 1. Values of R_1C_1 (grain), R_2C_2 (grain boundary), R_3C_3 (electrode), and L_1 corresponding to models shown using complex nonlinear least squares (CNLS) fitting for PZT

Model	T (K)	R_1 (kW)	C_1 (nF)	R_2 (kW)	C_2 (nF)	R_3 (kW)	C_3 (nF)	L_1(mH)
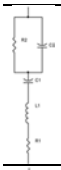	370	(0.028671 ± 0.00003)	(46.42 ± 0.001)	(2.712 ± 0.001)	(569.17 ± 0.01)	-	-	(0.3981 ± 0.0301)
	510	(0.027474 ± 0.00003)	(95.19 ± 0.001)	(1.469 ± 0.001)	(11.94 ± 0.01)	-	-	(0.4906 ± 0.015)
	538	(0.080273 ± 0.000139)	(20.24 ± 0.001)	(100.655 ± 0.186)	(385.46 ± 0.02)	-	-	(0.1806 ± 0.093)
	648	(0.089724 ± 0.000400)	(30.74 ± 0.001)	(0.848 ± 0.012)	(26.20 ± 0.01)	-	-	(0.3147 ± 0.05)
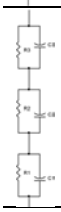	699	(757.143 ± 0.005)	(0.01783 ± 0.001)	(197.473 ± 0.005)	(0.2027 ± 0.001)	(758.60 ± 0.081)	(11.43 ± 0.001)	-
	748	(353.753 ± 0.003)	(0.01795 ± 0.001)	(51.321 ± 0.003)	(0.8542 ± 0.001)	(360.662 ± 0.008)	(5.262 ± 0.001)	-
	793	(113.862 ± 0.085)	(0.01906 ± 0.002)	(105.466 ± 0.185)	(1.054 ± 0.003)	(18.208 ± 0.171)	(0.576 ± 0.012)	-
	848	(229.175 ± 0.009)	(0.07200 ± 0.001)	(3634.91 ± 0.012)	(0.0258 ± 0.001)	(410.251 ± 0.010)	(4.112 ± 0.001)	-
	869	(190.388 ± 0.167)	(0.05.851 ± 0.001)	(1692. 99 ± 0.201)	(0.0294 ± 0.001)	(187.476 ± 0.136)	(6.041 ± 0.011)	-

by L_1 and C_1 respectively). The value of R_1 is estimated from the intercept of the Z″ vs. Z′ plot with the Z′ axis from Fig. 9(b). These estimated values of L_1, C_1 and R_1 are given in Table 2.

It is to be noted that the equivalent circuit model for this PZT at temperatures above T_c contains three parallel RC's connected in series which could be attributed to the grain, grain-boundary and electrode interface where the RC with the smallest time constant (R_1C_1) represents the grain whereas the RC with the largest time constant (R_3C_3) represents the electrode. This choice of model to represent the PZT behavior above T_c is acceptable since the PZT no longer remains piezoelectric above T_c and behaves as a normal dielectric. Below T_c the PZT is piezoelectric, indicating that the models representing grain and grain-boundary may change whereas the model representing the electrode may not change drastically. Therefore it might be advisable to consider a model containing a series $L_1C_1R_1$ circuit connected in series with a parallel RC circuit in which the values of R and C are close to R_3 and C_3 respectively. We denote this RC by $R_{2p}C_{2p}$. Since the material behaves differently below T_c the values of R_{2p} and C_{2p} may be different from the corresponding values of R_3 and C_3 representing the electrode in the model above T_c. However the same values of R_3 and C_3 obtained for the model above T_c may be chosen as initial guesses for R_{2p} and C_{2p}. The values of the initial guesses for L_1, C_1, R_1, R_{2p} and C_{2p} obtained in this way are given in Table 2. The exact values of L_1, C_1, R_1, R_{2p} and C_{2p} for the model below T_c were determined by a complex non-linear least squares (CNLS) fitting [31]. These are given

Table 2. Values of initial guesses for R_1,C_1, L_1 and R_{2p}, C_{2p}.

	538 K	648 K
R_1	80 W	53 W
L_1	1.867×10^{-7} H	3.117×10^{-8} H
C_1	1.356×10^{-7} F	3.235×10^{-7} F
R_{2p}	5.5×10^{5} W	5.5×10^{5} W
C_{2p}	3.979×10^{-9} F	3.979×10^{-9} F

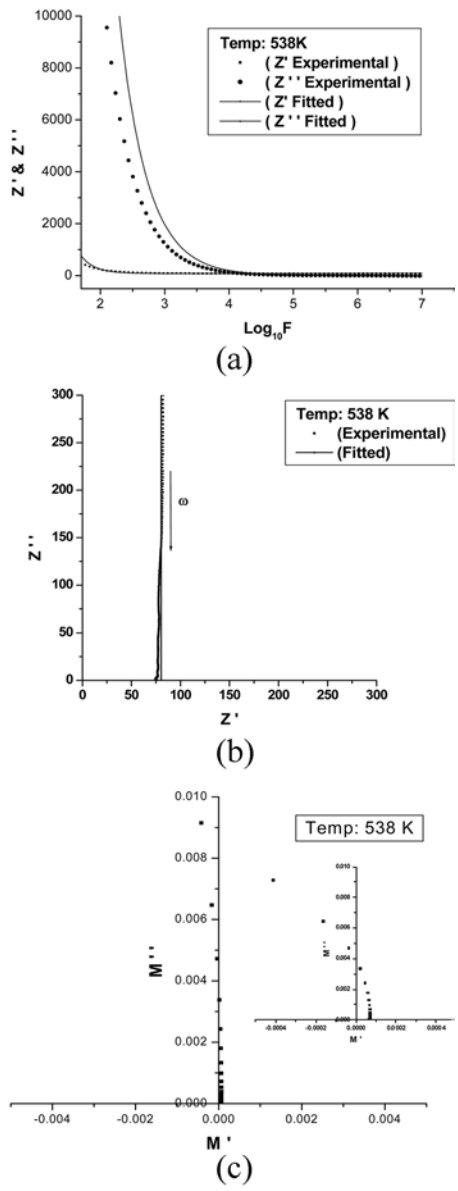

Fig. 9. Experimental and fitted plots for 538 K (a) Z' & Z'' vs. Log_{10} F; (b) Z'' vs. Z'.
(c) Experimental M'' vs. M' plot for 538 K. The inset shows the plot with changed scales to high light the pattern.

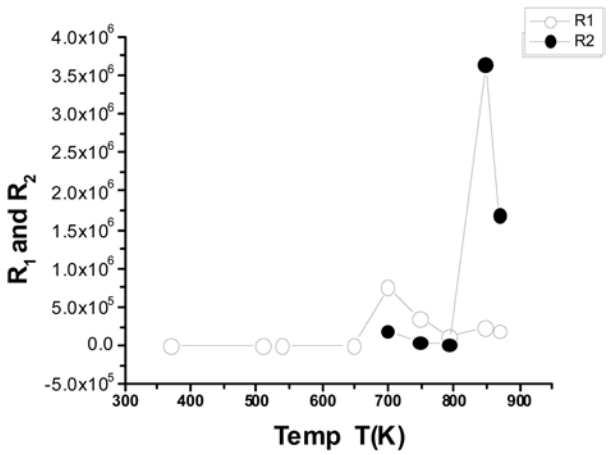

Fig. 10. Plot of grain (R_1), grain-boundary (R_2) resistances vs. temperature.

in Table 1 together with the corresponding models.

It is to be noted that the model for the PZT for temperatures below T_c contains a series LCR circuit only (the R_{2p} and C_{2p} discussed in the preceding paragraph correspond to the sample -electrode interface). Thus it is similar to the widely used Butterworth- Van Dyke model where the parallel capacitance (C_{12} of Fig. 5(a) is negligibly small. The system below T_c can still be treated as a grain- grain boundary -electrode system. Here we have a ceramic sample where grains are piezoelectric and the grain boundaries need not be so. We can estimate the resonance frequency of a PZT sample from its density, elastic constant and thickness. For a PZT grain of density, say, $\rho \sim 6 \times 10^3$ Kgm^{-3}, elastic stiffness constant $C_{33}D \sim 10^{10}$ and thickness t~5 micrometres [13] the resonance frequency $f \sim (C_{33}/4\,\rho\, t^2)^{1/2}$ [13] comes out to be ~600 MHz which is much beyond the highest frequency used in the measurements. Therefore at frequencies used for impedance measurements reported in this paper, it is very unlikely that the piezoelectric response of the tiny grains is being probed. It means that below T_c the whole sample behaves as a single resonator that is responding to the applied ac excitations. Also below T_c the sample resistance is found to be much smaller than the corresponding values above T_c. This is reasonable as flow of current is possible due to piezoelectric vibrations. The variation of R_1 obtained for the models above and below T_c with temperature is shown in Fig. 10. Similarly the variation of grain boundary resistance (R_2 from the model above T_c) as a function of temperature is also shown in this figure. The figure clearly reveals that the resistance vs. temperature slope for R_1 is positive above T_c. This is the so called PTCR behavior observed in ferro-electrics. The value of the grain boundary resistance above T_c increases above 575 K.The reason for rise in the values of grain-boundary resistances at a higher temperature than T_c is not known.

Conclusions

Impedance spectroscopic studies of a piezoelectric ceramic lead zicronate titanate (PZT) with a composition $PbZr_{1-x}Ti_xO_3$ (x = 0.4) has been carried out. Equivalent circuit models representing the experimental impedance data below and above the ferroelectric- to- paraelectric transition temperature T_c were obtained. It was found that a model comprising three parallel RC circuits connected in series represents the data best at temperatures above T_c. At temperatures below T_c a model consisting of a series LCR circuit connected in series with a parallel RC combination is found to represent the data best. This is consistent with the fact that above T_c the material behaves as an ordinary dielectric and the RC's appearing in the model may be taken to representing grain, grain-boundary and electrode processes. Also at temperatures below T_c, the PZT is piezoelectric (ferroelectric) and the series LCR may be taken to represent the sample and the further connected parallel RC may be taken to represent the electrode. Values of the components have been obtained.

References

1. A.J. Moulson and J.M. Herbert, "Electro-Ceramics" (Chapman and Hall, New York, 1990) p.294.
2. B. Jaffe, W.R. Cook Jr. and H. Jaffe, "Piezoelectric Ceramics" (Academic Press, London ,1971).
3. H.M.S. Georgiou and R. B. Mrad, Mechatronics 14, (2004) 667-674.
4. T.L. Jordan and Z. Ounaies, ICASE Report no, 2001-28, NASA/CR 2001-211225 (2001).
5. S.M. Gupta, N.V. Prasad and V.K. Wadhawan, Ferroelectrics 326 (2005) 43-47.
6. J. Cho, M. Anderson, R. Richards, D. Bahr and C. Richards, J. Micromech. Microeng. 15 (2005) 1804-1809.
7. J.S. Kim, K. Choi and I. Yu, IEEE Trans. Ultrasonics, Ferroelectrics and Frequency control 40 (1993) 424-426.
8. http://www.e-basteln.de/index_m.htm accessed on Jan. 23, 2010.
9. K.S. Van Dyke, Inst. Radio Engineers (IRE) Proc. 16 (1928) 742-764.
10. K.S. Van Dyke, Phys. Rev. 25 (1925) 895.
11. K.S. Van Dyke, Phys. Rev. 40 (1932) 1026.
12. W.P. Mason, Inst. Radio Engineers (IRE) Proc. 23 (1935) 1252-1263.
13. S. Sherrit, H.D. Wiedarick, B.K. Mukherjee and M. Sayer, J. Phys. D: Appl. Phys. 30 (1997) 2354-2363.
14. J.R. Macdonald in "Impedance Spectroscopy" (John Wiley and Sons, New York, 1987) p.13.
15. A.K. Jonscher in "Dielectric Relaxation in Solids" (Chelsea Dielectric Press, London ,1983) p.81.
16. H. Fricke, Philos. Mag.14 (1932) 310-318.
17. K.S. Cole and R.H. Cole, J. Chem. Phys. 9 (1941) 341-351.
18. R.K. Katare in "Application of Impedance Spectroscopy in the study of Electronic Ceramics" (Ph.D. Thesis, Rani Durgavati University, Jabalpur, India ,1997).
19. L. Pandey, O. Parkash, R.K. Katare and D. Kumar, Bull. Matter. Sci. 18 (1995) 563-576.
20. L .Pandey, R.K. Katare, O. Parkash and D. Kumar, Bull. Mater. Sci. 20 (1997) 933-947.
21. R.K. Katare, L. Pandey, R.K. Dwivedi, O. Parkash and D. Kumar, Ind. J. Engg. & Mater. Sci. 6 (1999) 34-42.
22. R.K. Katare, L. Pandey, O.P. Thakur, O. Parkash and D. Kumar, Modern Phys. Lett. B 17[8] (2003) 339-346.

23. R.K. Katare, L. Pandey, O.P. Thakur, O. Parkash and D. Kumar, Intl. J. Modern Phys. 19 (2005) 1783-1791.
24. V. Kumar, O.P. Thakur, L. Pandey, A. P. Guimaraes, A. Goel, O. Parkash and D. Kumar, Modern Phys. Lett. B 19 (2005) 697-706.
25. L. Pandey, R.K. Katare, O. Parkash, D. Kumar and O.P. Thakur, Ind. J. Pure & Appl. Phys. 36 (1998) 228-235.
26. V. Kumar in "NMR and Impedance spectroscopic Studies in Electronic Ceramics", (Ph.D. Thesis, Rani Durgavati University, Jabalpur, India, 2005).
27. P. Chaitanya in "Impedance Spectroscopy and rf Pulse Response of Piezoelectric Materials" (Ph.D. Thesis Rani Durgavati University, Jabalpur, India, 2008).
28. W.G. Caddy in "Piezoelectricity" (McGraw Hill Book co., New York, 1946) p.333
29. "The Radio Amateur's Hand-Book" (The American Radio League Inc.,1972) p.51.
30. M. Aparna, T. Bhimasankaram, S.V. Suryanarayana, G. Prasad and G.S. Kumar, Bull. Mater. Sci. 24 (2001) 497-504.
31. L. Pandey, in Workshop on use of computer in teaching Physics, partly sponsored by ICTP, Jabalpur, India (1992).